Indian Journal of Pure & Applied Physics
Vol. 55, October 2017, pp. 754-763

Study of buoyancy driven free convective flow of a micropolar fluid through a darcy-forchheimer porous medium with mutable thermal conductivity

S Rawat[a]*& S Kapoor[b]

[a]Department of General Studies, Jubail University College, Jubail Industrial City 31961, Kingdom of Saudi Arabia

[b]Department of Education in Science and Mathematics, Regional Institute of Education
(National council of Education Research and Training), Bhubaneshwar 751 022, India

Received 31 May 2016; accepted 12 June 2017

This paper presents a study of the natural convection flow, heat and mass transfer of an incompressible micropolar fluid between two vertical parallel plates containing a Darcy-Forchheimer porous medium. Asymmetric wall temperatures and concentrations are present and take into account a temperature-dependent thermal conductivity. The transformed equations for linear momentum, angular momentum, energy and species have been solved numerically using the finite element method. The effects of Darcy number (Da), Forchheimer number (Fs), Grashof number (Gr) and thermal conductivity parameter (S) on the velocity, angular velocity and temperature profiles have been studied in detail. The numerical results indicate that velocity and angular velocity (micro-rotation) increase as the Darcy number increases but they are reduced with increasing Forchheimer parameter, Grashof number and thermal conductivity parameter. Moreover, the thermal conductivity parameter increases as the temperature decreases. The effect of vortex viscosity parameter, R, on the volume flow rate, the total heat rate and the total species rate added to the fluid has also been examined. The effect of thermal conductivity parameter, S, on heat transfer rate has also been studied. A comparison with another method has also been presented and has been found to be well in agreement.

Keywords: Micropolar fluid, Porous medium, Variable conductivity, Finite element, Grashof number, Heat/mass transfer

1 Introduction

Natural convection in fluid saturated porous media constitutes an area of major activity in transport phenomena research owing to its application in a diverse number of fields including geothermal energy systems, enhanced recovery in petroleum reservoirs, filtration sciences, heat exchange between soil and atmosphere, transport of moisture through porous industrial materials and ceramic processing. The fundamental importance of convective flow in porous media has been well-reviewed in the recent book by Ingham and Pop[1]. Nield and Bejan[2] have also addressed in detail the natural convective flows due to combined buoyant mechanisms in porous media. Rawat and Kapoor[3] focused to develop a mathematical model for the comparative study of combined effects of free convective heat and mass transfer on the steady two-dimensional, laminar fluid flow past a moving permeable vertical surface subjected to a transverse uniform magnetic field.

Although, considerable work has been reported on flow heat and mass transfer in geometries with and without porous media[4,5], a majority of porous studies[6-8] have been on Darcy's law which states that the volume averaged velocity is proportional to the pressure gradient. Darcy's law however is valid only for slow (viscous-dominated) flows through porous media with low permeability. At higher flow rates or in highly porous media, there is a departure from the linear law and inertial effects become important. Physically, this departure is believed to be due to flow separation within the medium, whilst mathematically, it manifests itself as a nonlinear term in the velocity-pressure gradient relationship.

Recently, Rawat *et al.*[9] presented for the steady, two-dimensional magneto-convection heat transfer of a two-phase, electrically-conducting, particle-suspension in a channel containing a non-Darcian porous medium intercalated between two parallel plates, in the presence of a transverse magnetic field. The channel walls are assumed to be isothermal but at different temperatures. Rawat *et al.*[10] also investigate the two dimensional flow, heat and mass transfer of chemically reacting micro polar fluid over a non-linear stretching sheet with variable heat flux in a non-Darcy porous medium. The rate of chemical reaction is

*Corresponding author (E-mail: sam.rawat@gmail.com)

assumed to be constant throughout the fluid, i.e., homogenous.

The inability of classical (Newtonian) continuum mechanics to explain phenomena exhibited by fluids with suspended particles leads to the development of theory of micro polar fluids. This theory, presented by Eringen[11,12] includes the effect of local inertia and couple stresses and provides a physically and analytically robust mathematical model for simulating non-Newtonian characteristics exhibited by various polymeric fluids, colloidal suspensions, contaminated gases, blood, sediments etc. An excellent summary of these and other applications is available in the review by Ariman *et al.*[13]. Micro polar theory has therefore generated a considerable amount of interest and a wide spectrum of engineering problems. Rawat and Bhargava[14] presented the viscous, incompressible heat and mass transfer of a micro polar fluid through a Darcian porous medium in the presence of viscous heating and wall transpiration.

It is well known that some fluid properties like viscosity and thermal conductivity vary with temperature, so to accurately predict the flow and heat transfer processes in such fluids, it is necessary to incorporate the variation in physical properties with temperature in any model. The earliest known theoretical treatment of variable property effects along a vertical isothermal plate is the perturbation analysis of Hara[15] for air. Beg *et al.*[16] presented a solution scheme for the hydromagnetic boundary layer heat and mass transfer past a transpiring flat surface for thermophoresis and thermal conductivity variation. The pulsatile hydromagnetic flow and heat transfer of a non-Newtonian biofluid through a saturated non-Darcian porous medium channel with viscous heatingwas examined by Rawat *et al.*[17]. Mahmoud[18] studied the influence of temperature dependent thermal conductivity of a micropolar fluid with power-law variation in surface temperature.

Since, most of these studies were confined to purely fluid regimes neglecting the mutability of vital fluid properties, the present investigation therefore not only aims to extend the work of Cheng[19] but also to study numerically the natural convection heat and mass transfer of a fully developed micropolar fluid flow in a Darcy-Forchheimer porous medium for asymmetric wall temperatures and concentrations with temperature-dependent thermal conductivity. Such a study, to the authors' knowledge has not yet appeared in the literature despite immediate applications in packed-bed chemical reactors, polymer processing, grain storage, insulation of building and purification of crude oil etc. The governing partial differential equations for the flow are transformed and solved using Finite element method. The model finds applications in polymer technology, aerodynamic heating, geophysics and ceramic processing.

2 Mathematical Models

Consider the laminar natural convection flow between two vertical plates in a homogenous, incompressible, micropolar fluid-saturated porous medium with temperature dependent thermal conductivity. The vertical plates are separated by a distance b with reference to an x, y coordinate system, where the x-axis is directed along the vertical plates and the y-axis is transverse to this. It is assumed that the two walls are maintained at different temperatures and concentrations resulting in an asymmetric situation with respect to temperature and concentration, respectively. The flow is also assumed steady and fully developed, i.e., transverse velocity is zero and therefore the flow depends only on the transverse coordinate, y. The geometry of the system is shown in Fig. 1. Neglecting viscous heating and thermal dispersion effects, under the Boussinesq approximation, the one-dimensional conservation equations may be presented as follows:

Linear momentum equation:

$$(\mu+\kappa)\frac{d^2u}{dy^2}+k\frac{dg}{dy}+\rho\beta_T g_a(T-T_0)+\rho\beta_C g_a (C-C_0)-\frac{(\mu+\kappa)}{k_p}u-\frac{b_F\rho}{k_p}u^2=0 \quad \ldots (1)$$

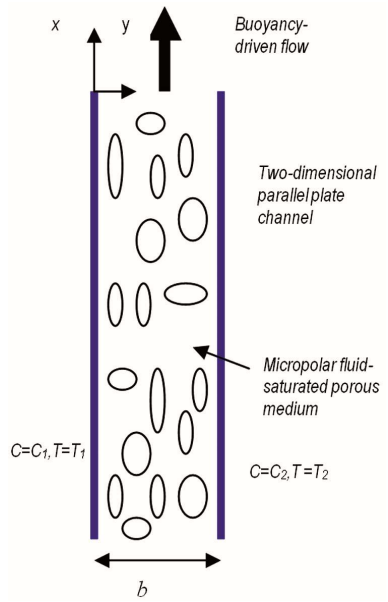

Fig. 1 — Physical model and co-ordinate system.

Angular momentum equation:

$$\gamma\frac{d^2g}{dy^2} - k(2g + \frac{du}{dy}) = 0 \quad \ldots (2)$$

Energy equation:

$$\frac{d}{dy}\left(k_f \frac{dT}{dy}\right) = 0 \quad \ldots (3)$$

Diffusion equation:

$$\frac{d^2C}{dy^2} = 0 \quad \ldots (4)$$

The corresponding boundary conditions on the vertical surfaces are

$$y = 0 : u = 0, g = 0, T = T_1, C = C_1 \quad \ldots (5a)$$
$$y = b : u = 0, g = 0, T = T_2, C = C_2 \quad \ldots (5b)$$

where μ, κ, k_p and b_F designate the newtonian dynamic viscosity, eringen vortex viscosity, permeability and inertia coefficient of the porous medium, respectively. $\gamma = \left(\mu + \frac{\kappa}{2}\right)j$, is the spin gradient viscosity, i.e., gyro-viscosity, j denotes the microinertia density, u is the micropolar linear velocity, g is the angular velocity (micro-rotation) of the micropolar fluid micro-elements, k_f is the thermal conductivity of the fluid, T and C are the fluid temperature and concentration, respectively, T_0 is the inlet temperature and C_0 is the inlet concentration. The left plate (i.e, at $y = 0$) is kept at constant temperature T_1 and the right plate (i.e., at $y = b$) is maintained at a constant temperature T_2. Additionally, the concentration varies from C_1 on the left plate to C_2 on the right plate.

We also note that the micro-rotation conditions imposed at both plates correspond to the case where particle rotation (spin) at the wall is not permitted, i.e., micro-element rotation vanishes. Such a scenario corresponds physically to concentrated particle flows, as described by Gorla *et al.*[20]. We further assume that the thermal conductivity is a function of temperature and is defined as:

$$k_f = k_1[1+\propto (T - T_0)] \text{ or } k_f = k_1[1 + S\theta] \quad \ldots (6)$$

where $S = \alpha(T_1 - T_0)$

where, k_1 is the fluid thermal conductivity at temperature T_1 and α is a constant depending on the nature of the fluid. In general, S > 0 for water and air whereas, S > 0 for fluids such as lubricating oils. Proceeding with the analysis, we introducing the similarity transformations:

$$u = \frac{\mu Gr}{b\rho}, y = Yb, g = \frac{\mu Gr}{b^2\rho}H, \theta = \frac{T-T_0}{T_1-T_0}, \Phi = \frac{C-C_0}{C_1-C_0} \quad \ldots (7)$$

Substitution into Eqs (1) – (5) leads to the following set of non-linear, coupled, ordinary differential equations:

Linear momentum equation:

$$(1+R)\frac{d^2U}{dY^2} + R\frac{dH}{dY} + \theta + N\Phi - \frac{(1+R)}{Da}U - \frac{FsGr}{Da}U^2 = 0 \quad \ldots (8)$$

Angular momentum equation:

$$\left(1 + \frac{R}{2}\right)\frac{d^2H}{dY^2} - BR\left(2H + \frac{dU}{dY}\right) = 0 \quad \ldots (9)$$

Energy equation:

$$(1 + S\theta)\frac{d^2\theta}{dY^2} + S(\frac{d\theta}{dY})^2 = 0 \quad \ldots (10)$$

Diffusion equation:

$$\left(\frac{d^2\Phi}{dY^2}\right) = 0 \quad \ldots (11)$$

where, $B = \frac{b^2}{j}$ and $R = \frac{\kappa}{\mu}$ are micropolar parameters (dimensionless material properties) and $N_b = \frac{\beta_C(C_1-C_0)}{\beta_T(T_1-T_0)}$ is the buoyancy ratio, $Gr = \frac{g_a\beta_T b^3\rho^2}{\mu^2}(T_1 - T_0)$ is the Grashof number, $Da = \frac{K_p}{b^2}$ is the Darcy number and $Fs = \frac{b_F}{b}$ is the Forchheimer (quadratic porous drag) number. The transformed boundary conditions now become:

$$\text{At } Y = 0 : U = 0, H = 0, \theta = 0, \Phi = 1 \quad \ldots (12)$$

$$\text{At } Y = 1 : U = 0, H = 0, \theta = m, \Phi = n \quad \ldots (13)$$

where, $m = \frac{T_2-T_0}{T_1-T_0}$ is the wall temperature ratio and $n = \frac{C_2-C_0}{C_1-C_0}$ is the wall concentration ratio of special significance in engineering applications is the shear stress, the wall heat flux and wall heat transfer coefficient. The shear stress at the left wall is given by:

$$\tau_1 = [(\mu + \kappa)\left(\frac{du}{dy}\right) + \kappa g]_{y=0} = \frac{(\mu+\kappa)Gr\mu}{\rho b^2}U'(0) \quad \ldots (14)$$

The heat flux at the left wall may be written using Fourier's law as follows:

$$q_1 = -k_f \frac{dT}{dy}\Big|_{y=0} = -\frac{k_f(T_1-T_0)}{b}\theta'(0) \quad \ldots (15)$$

The heat transfer coefficient at the left wall is given by:

$$h_1 = \frac{q_1}{(T_1-T_0)} = -\frac{k_f}{b}\theta'(0) \quad \ldots (16)$$

The Nusselt number at the left wall can be defined thus:

$$Nu = \frac{h_1 b}{k_f} = -\theta'(0) \quad \ldots (17)$$

The dimensionless volume flow rate is given by:

$$Q = \int_0^1 U dY \quad \ldots (18)$$

The dimensionless total heat rate added to the fluid is given by:

$$E = \int_0^1 U\theta dY \quad \ldots (19)$$

Finally the dimensionless total species rate added to the fluid is given by:

$$\varphi = \int_0^1 U\Phi dY \quad \ldots (20)$$

Additionally the wall couple stress at both plates can be defined by:

$$M_w = \left[\gamma \frac{\partial g}{\partial y}\right] \text{ at } y = 0 \text{ (left plate) and}$$
$$M_w = \left[\gamma \frac{\partial g}{\partial y}\right] \text{ at } y = 1 \text{ (right plate)} \quad \ldots (21)$$

3 Numerical Solution by Finite Element Method

The transformed two-point boundary value problem defined by Eqs (8) – (13) is solved using finite element method. Details of the method are given in Reddy[21] and Bathe[22]. The whole domain is divided into a set of 81 line elements of equal width, each element being two noded.

3.1 Variational formulation

The variational form associated with Eqs (8) - (11) over a typical two noded linear element (Y_e, Y_{e+1}) is given by:

$$\int_{Y_e}^{Y_{e+1}} w_1 \left\{(1+R)\frac{d^2U}{dY^2} + R\frac{dH}{dY} + \theta + N\Phi - \frac{(1+R)}{Da}U - \frac{FsGr}{Da}U^2\right\} dY = 0 \quad \ldots (22)$$

$$\int_{Y_e}^{Y_{e+1}} w_2 \left\{\left(1+\frac{R}{2}\right)\frac{d^2H}{dY^2} - BR\left(2H + \frac{dU}{dY}\right)\right\} dY = 0 \quad \ldots (23)$$

$$\int_{Y_e}^{Y_{e+1}} w_3 \left\{(1+S\theta)\frac{d^2\theta}{dY^2} + S\left(\frac{d\theta}{dY}\right)^2\right\} dY = 0 \quad \ldots (24)$$

$$\int_{Y_e}^{Y_{e+1}} w_4 \left\{\frac{\partial^2\Phi}{\partial Y^2}\right\} dY = 0 \quad \ldots (25)$$

where w_1, w_2, w_3 and w_4 are arbitrary test functions and may be viewed as the variation in U, H, θ and ϕ respectively.

3.2 Finite element formulation

The finite element model may be obtained from Eqs (22)-(25) by substituting finite element approximations of the form:

$$U = \sum_{j=1}^{2} U_j \psi_j, H = \sum_{j=1}^{2} H_j \psi_j,$$
$$\theta = \sum_{j=1}^{2} \theta_j \psi_j, \Phi = \sum_{j=1}^{2} \theta_j \psi_j \quad \ldots (26)$$

with $w_1 = w_2 = w_3 = w_4 = \psi_i (i = 1, 2)$ where ψ_i are the shape functions for a typical element (Y_e, Y_{e+1}) and are taken as::

$$\psi_1^{(e)} = \frac{Y_{e+1} - Y}{Y_{e+1} - Y_e}, \psi_2^{(e)} = \frac{Y - Y_e}{Y_{e+1} - Y_e}, (Y_e \le Y \le Y_{e+1}) \quad \ldots (27)$$

The finite element model of the equations for a typical element (Y_e, Y_{e+1}) for U, H, θ and Φ thus formed is given by:

$$\begin{bmatrix} [K^{11}][K^{12}][K^{13}][K^{14}] \\ [K^{21}][K^{22}][K^{23}][K^{24}] \\ [K^{31}][K^{32}][K^{33}][K^{34}] \\ [K^{41}][K^{42}][K^{43}][K^{44}] \end{bmatrix} \begin{bmatrix} \{U\} \\ \{H\} \\ \{\theta\} \\ \{\Phi\} \end{bmatrix} = \begin{bmatrix} \{b^1\} \\ \{b^2\} \\ \{b^3\} \\ \{b^4\} \end{bmatrix} \quad \ldots (28)$$

where $[K^{mn}]$, and $[b^m]$ (m, n=1, 2, 3, 4) are the matrices of order 2×2 and 2×1, respectively. All these matrices may be defined as follows:

$$K_{ij}^{11} = -(1+R)\int_{Y_e}^{Y_{e+1}} \frac{d\psi_i}{dY}\frac{d\psi_j}{dY} dY - \frac{(1+R)}{Da}\int_{Y_e}^{Y_{e+1}} \psi_i \psi_j dY$$
$$-\frac{FsGr}{Da}\overline{U_1}\int_{Y_e}^{Y_{e+1}} \psi_i \psi_1 \psi_j dY - \frac{FsGr}{Da}\overline{U_2}\int_{Y_e}^{Y_{e+1}} \psi_i \psi_2 \psi_j dY$$
$$K_{ij}^{12} = R\int_{Y_e}^{Y_{e+1}} \psi_i \frac{d\psi_j}{dY} dY$$
$$K_{ij}^{13} = \int_{Y_e}^{Y_{e+1}} \psi_i \psi_j dY$$
$$K_{ij}^{14} = N_b \int_{Y_e}^{Y_{e+1}} \psi_i \psi_j dY$$
$$K_{ij}^{21} = -BR\int_{Y_e}^{Y_{e+1}} \psi_i \frac{d\psi_j}{dY} dY$$
$$K_{ij}^{22} = -\left(1+\frac{R}{2}\right)\int_{Y_e}^{Y_{e+1}} \frac{d\psi_i}{dY}\frac{d\psi_j}{dY} dY - 2BR\int_{Y_e}^{Y_{e+1}} \psi_i \psi_j dY$$
$$K_{ij}^{23} = K_{ij}^{24} = 0,$$
$$K_{ij}^{31} = K_{ij}^{32} = 0$$
$$K_{ij}^{33} = -\int_{Y_e}^{Y_{e+1}} \frac{d\psi_i}{dY}\frac{d\psi_j}{dY} dY - S\overline{\theta_1}\int_{Y_e}^{Y_{e+1}} \psi_1 \frac{d\psi_i}{dY}\frac{d\psi_j}{dY} dY$$
$$-S\overline{\theta_2}\int_{Y_e}^{Y_{e+1}} \psi_2 \frac{d\psi_i}{dY}\frac{d\psi_j}{dY} dY$$
$$K_{ij}^{34} = 0$$
$$K_{ij}^{41} = K_{ij}^{42} = K_{ij}^{43} = 0$$

$$K_{ij}^{44} = -\int_{Y_e}^{Y_{e+1}} \frac{d\psi_i}{dY}\frac{d\psi_j}{dY}dY$$

$$b_i^1 = -\left(\psi_i \frac{dU}{dY}\right)_{Y_e}^{Y_{e+1}},\ b_i^2 = -\left(\psi_i \frac{dH}{dY}\right)_{Y_e}^{Y_{e+1}}$$

$$b_i^3 = -\left(\psi_i \frac{d\theta}{dY}\right)_{Y_e}^{Y_{e+1}} - s\overline{\theta_1}\left(\psi_1\psi_i \frac{d\theta}{dY}\right)_{Y_e}^{Y_{e+1}} - s\overline{\theta_2}\left(\psi_2\psi_i \frac{d\theta}{dY}\right)_{Y_e}^{Y_{e+1}}$$

$$b_i^4 = -\left(\psi_i \frac{d\Phi}{dY}\right)_{Y_e}^{Y_{e+1}} \quad \ldots (29)$$

Where

$$\overline{U} = \sum_{i=1}^{2} \overline{U}_i\psi_i\ ,\ \overline{\theta} = \sum_{i=1}^{2} \overline{\theta}_i\psi_i \quad \ldots (30)$$

Each element matrix is of the order 8×8. Since the whole domain is divided into a set of 81 line elements. Thus after assembly of all the elements equations we obtain a matrix of order 328 × 328. This system of equations as obtained is non-linear therefore an iterative scheme has been used to solve it. The system is linearized by incorporating the functions $\overline{U}$ and $\overline{\theta}$, which are assumed to be known. After applying the given boundary conditions, only a system of 320 equations remains for the solution which has been solved by the Gauss-Seidel method maintaining an accuracy of 0.0005.

4 Results and Discussion

Figures 2-14 illustrate a selection of the numerical results obtained for the variation of the six main flow parameters, Da, Fs, Gr, R, N_b, S. Default parameter values have been prescribed as $N_b = 2$, $B = 1$, $m = 0.2$, $n = 0.1$ for the finite element computations. These values are used throughout the computations, unless otherwise indicated. These figures are obtained to illustrate the influence of the Darcy number, porous medium inertia coefficient, Grashof number, vortex viscosity parameter, buoyancy ratio and variable thermal conductivity parameter on the flow, temperature and species distributions across the channel width.

Figures 2 and 3 display results for the velocity U and angular velocity H distribution versus Y for different values of Darcy number Da. Darcy number is directly proportional to the permeability of the porous medium, so as Da increases, the bulk matrix (Darcian) decreases and therefore an increase in translational velocity of the micropolar fluid as shown by Fig. 2. With increasing permeability the porous matrix structure becomes less and less prominent and in the limit of infinite Da values, the medium porosity vanishes. Obviously a high porosity porous medium exerts less resistance to flow. Hence the micropolar fluid is accelerated, i.e., translational momentum is boosted, with the rise in Da, explaining the ascent in U values. In Fig. 3, we observe that values of micro-rotation are negative in the first half whereas in the second half, these are positive, thus showing a reverse rotation near the two boundaries. Close examination of Fig. 3 reveals that micro-rotation, H, actually vanishes in the zone, $0.25 < H < 0.375$, and this vanishing location drifts closer to the centre-line of the channel as Da values increase from 0.05 through 0.1, 0.5, 1 and 2.

Micro-elements therefore do not perform rotary motions as the curves cross the Y axis. An increase in the Darcy number leads to an increase in micro-rotation. So the porosity of the medium can be used effectively to increase or decrease the angular rotation commonly arising in suspension flows in porous lubrication problems, e.g., porous journal bearings[23]. We note that for the limiting case of $Da \to \infty$, the fibers of the porous matrix vanish and the regime becomes purely fluid i.e. infinite permeability (hydraulic conductivity).

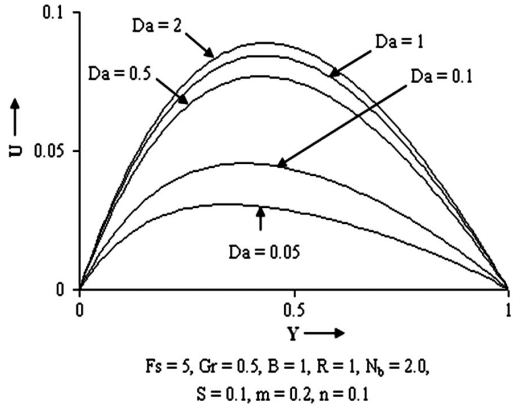

Fig. 2 — U versus Y for various Da values.

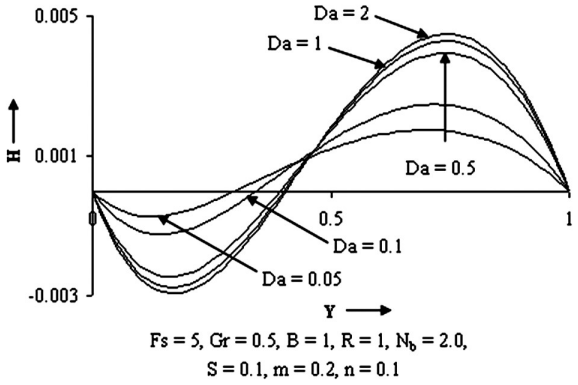

Fig. 3 — H versus Y for various Da values.

Figures 4 and 5 show the effect of Forchheimer (inertial porous) parameter on the translational and angular velocity profiles. For the case of $Fs = 0$ the regime is Darcian. A rise in *Da* from 10 (weakly imposed quadratic drag) to 40, retards the flow development and decreases the velocity, *U*. In the Darcy-Forchheimer regime the flow becomes increasingly more chaotic in actual porous media and an inertial core region can develop, as highlighted by Dybbs and Edwards[24]. Figure 4 demonstrates that the microrotation decreases with the increase in inertial parameter *Fs*, though the variation is not very prominent.

Figure 6 shows the distribution of velocity *U* versus *Y* for various thermal Grashof numbers *Gr*, i.e., free convection parameter. As *Gr* increases from 0 to 10, velocity decreases. Clearly from Fig. 6, it is interesting to note that in the case of forced convection, i.e., $Gr = 0$, the velocity profile is maximized. Buoyancy therefore suppresses flow and induces deceleration in the channel, even for weak values of *Gr*.

The influence of vortex viscosity parameter *R* on velocity profiles and microrotation profiles is depicted in Figs 7 and 8. As *R* increases from 0 to 0.5, the magnitude of microrotation (*H*) tends to increase while the translational velocity decreases which is well verified by the results of Cheng[19]. The parameter, *R*, is proportional to vortex viscosity of the fluid micro-structure.

Increasing *R* therefore results in flow retardation in the linear velocity boundary layer (Fig. 7) as confirmed by our results and those of many other researchers including Rees and Pop[25], Rees and Bassom[26] and Chiu and Chou[27]. All velocity profiles are parabolic with a maximum around the channel centre line ($Y = 0$) and for $R = 0$ (Newtonian case) the magnitudes are the highest.

Therefore micropolar fluids decelerate flow owing to the presence of micro-elements, compared with Newtonian fluids. In Fig. 8, we observe that for $0 < Y < 0.4$ approximately, the *H* values are negative; all profiles cross the *Y* axis at $Y \sim 0.4$ and profiles follow a parabolic profile peaking at $Y \sim 0.75$ before descending to zero at $Y = 1$ (right plate). Maximum

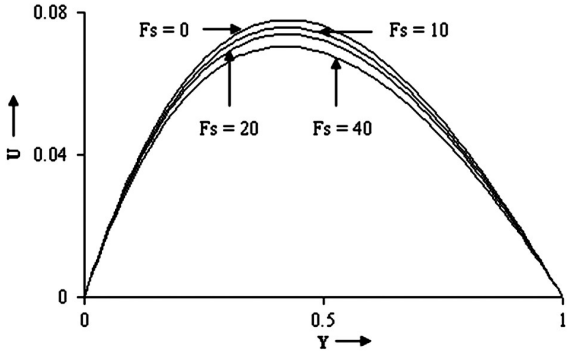

Fig. 4 — *U* versus *Y* for various *Fs* values.

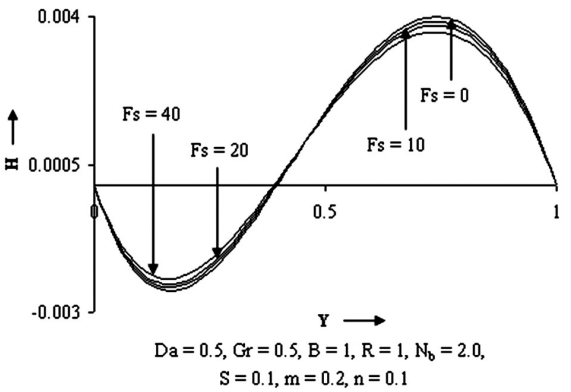

Fig. 5 — *H* versus *Y* for various *Fs* values.

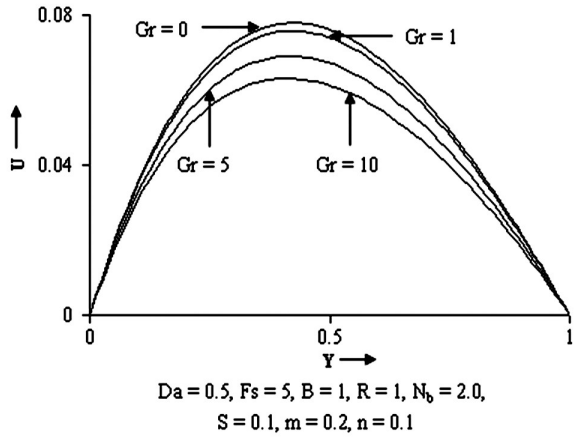

Fig. 6 — *U* versus *Y* for various *Gr* values.

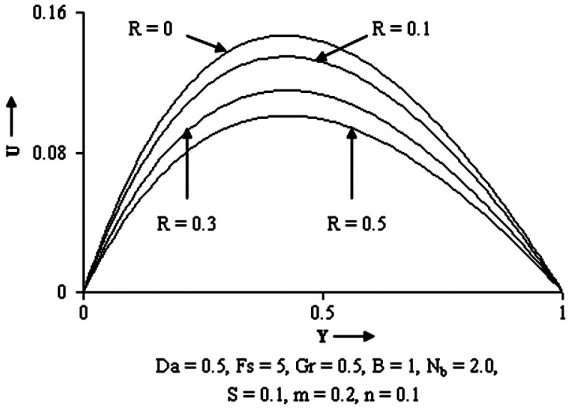

Fig. 7 — *U* versus *Y* for various *R* values.

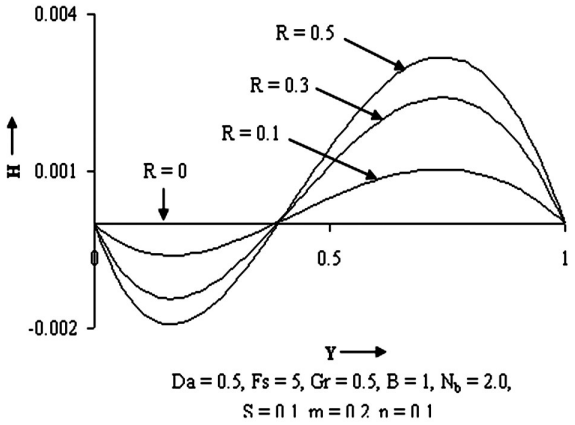

Fig. 8 — H versus Y for various R values.

H values are witnessed for R = 0.5 (maximum vortex viscosity parameter) indicating that with increasing gyroviscosity (vortex viscosity) fluid microelements spin faster.

Figures 9-11 provide distributions for the effect of thermal conductivity parameter on velocity, angular velocity and temperature profiles. $S = 0$ corresponds to the case, when the thermal conductivity κ of the fluid is constant (i.e, thermal conductivity is independent of temperature). Figure 9 indicates that an increase in thermal conductivity parameter, S, decreases the translational velocity. All profiles are skewed parabolas with peaks occurring prior to the centre-line of the channel. Micro-rotation profiles (Fig. 10) are also shown to decrease as S rises from 0 to 0.4; H values are negative for a section of the channel width, viz $0< Y < 0.4$, after which they become positive, indicating that micro-elements reverse in spin direction beyond this point. Maximum positive H values occur at $Y \sim 0.75$. Temperature function, θ, is similarly depressed by a rise in S values as shown in Fig. 11. For the constant thermal conductivity case, $S = 0$, we note that the profile is linear descending from a maximum at the left plate.

As S increases from 0 to 0.1, 0.2, 0.3, 0.4, the temperature profiles become increasingly steeper in the range $0 < Y< 0.25$, indicating that a higher S values induces a sharp decrease in temperature in the vicinity adjacent to the left plate. Further from the left plate however the profiles decrease in gradient and descend more gradually towards the right plate converging to a value of 0.2 as specified in the right plate thermal boundary condition (13). We note that these computations correspond to a weak free convection regime as Gr is set as 0.5.

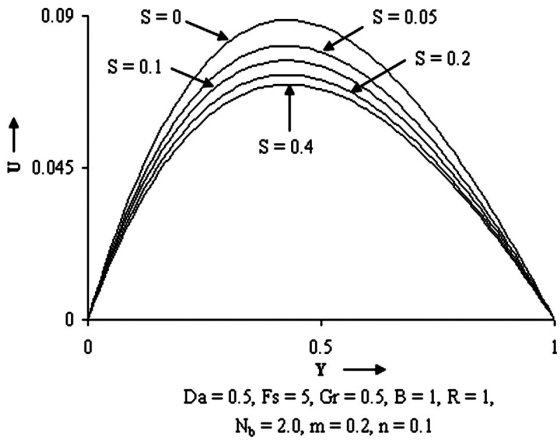

Fig. 9 — U versus Y for various S values.

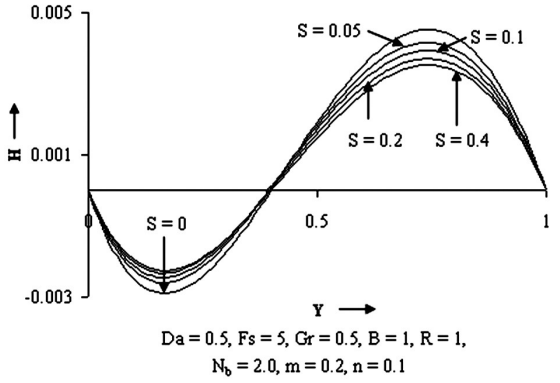

Fig. 10 — H versus Y for various S values.

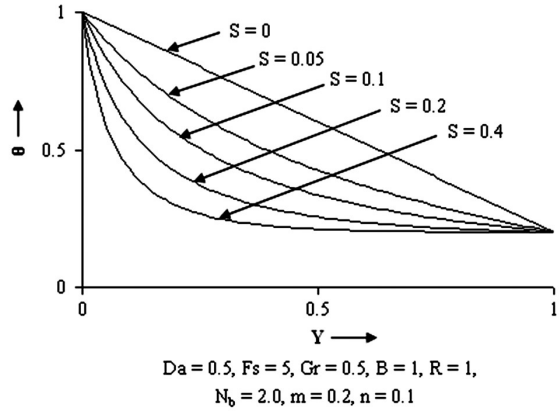

Fig. 11 — θ versus Y for various S values.

Figure 12 shows the effects of the buoyancy ratio N_b and vortex viscosity parameter R on the dimensionless volumerate Q. An increase in the buoyancy ratio, N_b, from 0 to 4 enhances the velocity of the fluid, thus increasing the volume flow rate Q of the fluid through the channel. However, an increase in the vortex viscosity parameter leads to a decrease in the

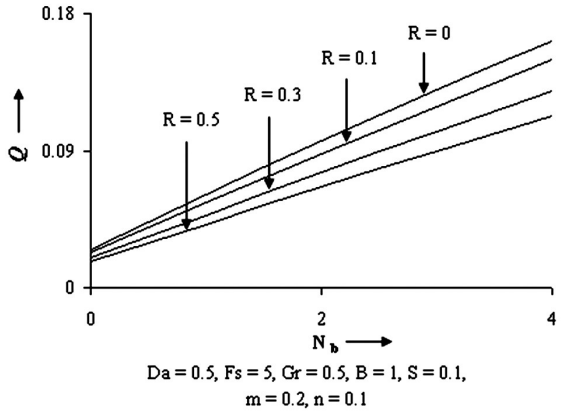

Fig. 12 —Q versus N_b for various R values.

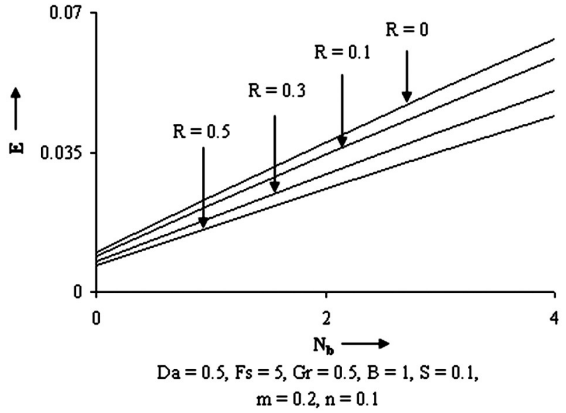

Fig. 13 — E versus N_b for various R values.

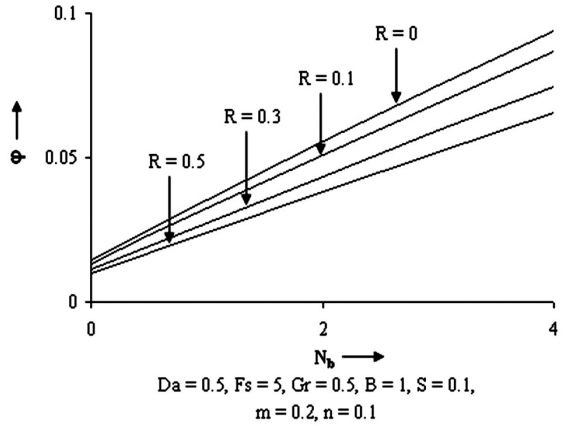

Fig. 14 — ϕ versus N_b for various R values.

volume flow rate through the channel, which is consistent with the decrease in linear velocity observed with a rise in R in Fig. 8. Q as shown in Eq. (18) is obtained by integrating linear velocity across the channel width $[Q=\int_0^1 UdY]$ indicating a direct proportionality between the volumetric flow rate and linear velocity field (hence the linear nature of the Q profiles).

Figure 13 plots the variation of the dimensionless total heat rate added to the fluid E with the buoyancy ratio N_b for various vortex viscosity parameters (R = 0,0.1, 0.3, 0.5). It is observed that an increase in buoyancy ratio leads to an increase in the fluid flow and so the heat transfer between the two vertical plates also increases which ultimately increases the total heat rate added to the fluid in the channel.

Equation (19) viz, $[E=\int_0^1 U\theta dY]$, indicates the linear relationship between E and U and θ, explaining again the linear profiles in Fig. 13. We also note that as the vortex viscosity parameter increases, the total heat rate added to the fluid decreases, indicating that micropolar fluids can serve as coolants in engineering processes, a fact established by many other investigations e.g. Gorla *et al,*[20]. Micro-structure clearly reduces heat transfer rates in the channel.

Finally the dimensionless total species rate added to the fluid volume, φ is plotted as a function of the buoyancy ratio N_b for different values of vortex viscosity parameters R, in Fig. 14. From equation (20),$\varphi = \int_0^1 U\Phi dY$, i.e., a direct linear relationship exists between φ and Φ. It is apparent that an increase in the buoyancy ratio increases the fluid flow which leads to an increase in the total species rate added to the fluid between the two vertical walls. Total species rate added to the fluid in the vertical channel also clearly decreases with an increase in vortex viscosity parameter, which as described earlier decreases the linear velocity field and therefore also φ.

We have also presented computations of the skin friction and wall heat transfer rates at the left plate, $U'(0)$ and$-\theta'(0)$ in Table 1.

We observe that increasing the thermal conductivity parameter, S, greatly increases the rate of heat transfer at the left wall. However the skin friction at the left wall is reduced with a rise in thermal conductivity parameter, i.e., the micropolar fluid is decelerated at the left plate with a rise in S from 0 to 0.4. It can be inferred therefore that the thermal conductivity parameter, S, is an effective means of controlling the rate of heat transfer as well as skin friction.

Further in order to verify the accuracy of the present computation, the same system of equations is solved using the finite difference method (methodology has been omitted for brevity, details are however available in Bhargava *et al.*[28]) and our results are shown in Table 2. Excellent correlation is observed between both methods for the chosen case of $Da = 1$ for the

Table 1 — Values of $U'(0)$ and $-\theta'(0)$ for different values of S Da=0.5, Fs=5, Gr=0.5, B=1, R=1, Nb=2.0,S=0.1, m=0.2, n=0.1

S	$U'(0)$	$-\theta'(0)$ (Nusselt number)
0.00	0.457353	0.80000
0.05	0.428868	2.18749
0.10	0.410347	3.74051
0.15	0.398009	5.27176
0.20	0.389244	6.73164
0.25	0.382794	8.11312
0.30	0.377834	9.41202
0.35	0.37389	10.6326
0.40	0.370811	11.7833

Table 2 — Comparison table of finite difference and finite element computations Fs=5, Gr=0.5, B=1, R=1, Nb=2.0, S=0.1, m=0.2, n=0

	U (Da = 1.0)		H (Da = 1.0)	
Y	FEM	FDM	FEM	FDM
0	0	0	0	0
0.0987654	0.0372309	0.037241	-0.00235333	-0.00235346
0.209877	0.064854	0.06490	-0.00262894	-0.0026298
0.320988	0.0798764	0.0798771	-0.00138019	-0.0013825
0.432099	0.0843658	0.084366	0.000558018	0.0005581
0.54321	0.0800585	0.0800589	0.00250234	0.00250241
0.654321	0.0684665	0.0684671	0.00388953	0.0038897
0.765432	0.0509448	0.0509462	0.00425315	0.00425336
0.876543	0.0287392	0.028745	0.0032061	0.003212
1	0	0	0	0

dimensionless velocity (U) profile and also for dimensionless micro-rotational (H) profile. Moreover our velocity and angular velocity profiles exactly match with those of Cheng[19] when $Da \to \infty, Fs = 0, S = 0$, i.e., for the constant thermal conductivity, non-porous version of our model equations, although we have not included numerical values for brevity. Therefore the present finite element solutions are highly accurate.

5 Conclusions

A mathematical model has been presented for free convective heat and mass transfer of a micropolar fluid flow between vertical parallel plates containing an isotropic, homogenous, non-Darcian porous medium The thermal conductivity of the micropolar fluid is temperature-dependent. The model has been transformed and rendered into dimensionless form and the resulting equations solved using the finite element method. Our numerical simulations have shown that:

(i) The translational velocity (U) increases with the increase in Darcy Number, Da, as well as wall temperature ratio (m). However it decreases with an increase in Forchheimer number Fs, Grashof number, Gr, and thermal conductivity parameter, S.

(ii) The angular velocity (micro-rotation, H) increases with a rise in Darcy Number, Da, and wall temperature ratio, m,. However it decreases with an increase in Forchheimer number, Fs, Grashofnumber,Gr, and thermal conductivity parameter (S).

(iii) The magnitude of microrotation, H, increases with the increase in vortex viscosity parameter, R, which substantially decelerates the flow in the channel.

(iv) The thermal conductivity parameter, S, and wall temperature ratio, m, can be used effectively for controlling the rise in temperature.

(v) The skin friction at the left plate, $U'(0)$ continuously decreases with the increase in thermal conductivity parameter, S, which shows that by increasing the thermal conductivity parameter, friction at the plate surface can be sufficiently reduced.

(vi) Heat transfer rate, $-\theta'(0)$ (Nusselt number), increases with an increase in thermal conductivity parameter, S. This parameter thereby can be employed to effectively control the rise in the temperature in practical industrial systems.

(vii) Our results also indicate that the micropolar fluids ($R > 0$) possess a lower volumetric flow rate, total heat rate added to the fluid, and the total species rate added to the fluid in comparison with Newtonian fluids ($R = 0$).

Nomenclature

b width of the channel
b_f inertial constant
C concentration
Da Darcy number
E dimensionless total heat rate added to the fluid
Fs Forchheimer number
g angular velocity
ga gravitational acceleration
Gr Grashof number
H dimensionless angular velocity
j microinertia density
k_f thermal conductivity
m wall temperature ratio
n wall concentration ratio
N_b buoyancy ratio
Nu Nussult number
Q dimensionless volume flow rate
R vortex viscosity parameter
S thermal conductivity parameter
T temperature
u velocity of the fluid
U dimensionless velocity of the fluid
y transverse coordinate
Y dimensionlesstransverse coordinate
μ dynamic viscosity
k vortex viscosity

ρ density
γ spin gradient viscosity
k_p permeability
θ dimensionless temperature
Φ dimensionless concentration
φ dimensionless total species rate added to the fluid

Subscripts
0 condition at the inlet
1 condition on the inner surface of the left plate
2 condition on the inner surface of the right plate

References

1 Ingham D B & Pop I, *Transport phenomena in porous media*, Vol II, (Pergamon: Oxford), 2002.
2 Nield D A & Bejan A, *Convection in porous media*, Second Edn, (Springer: New York), 1999.
3 Rawat S & Kapoor S, *Proc Eng*, 38 (2012) 2288.
4 Churchill S W & Chu H H S, *Int J Heat Mass Transfer*, 18 (1975) 1323.
5 Gorla R S R, *Physico-Chem Hydrodyn*, 1 (1980) 77.
6 Minkowycz W J & Cheng P, *Int J Heat Mass Transfer*, 19 (1987) 805.
7 Nakayama A & Koyama H, *Heat Mass Transfer J*, 28 (1995) 1041.
8 Badr H M & Pop I, *Int J Heat Mass Transfer*, 31 (1988) 2527.
9 Rawat S, Bhargava R, Kapoor S, Bég O A, Bég T A & Bansal R, *J Appl Fluid Mech*, 7 (2014) 249.
10 Rawat S, Kapoor S & Bhargava R, *J Appl Fluid Mech*, 9 (2016) 321.
11 Eringen A C, *J Math Mech*, 16 (1966) 1.
12 Eringen A C, *J Math Anal Appl*, 38 (1972) 480.
13 Ariman T, Turk M A & Sylvester N D, *Int J Eng Sci*, 11 (1973) 905.
14 Rawat S & Bhargava R, *Int J Appl Math Mech*, 5 (2009) 58.
15 Hara T, *Trans Jpn Soc Mech Eng*, 20 (1954) 517.
16 Beg O A, Zueco J, Rawat S & Ghosh S K, *Em J Eng Res*, 14 (2009) 59.
17 Rawat S, Bhargava S, Beg O A & Bhargava B R, *Em J Eng Res*, 14 (2009) 77.
18 Mohmoud M A A, *Physica A*, 375 (2007) 401.
19 Cheng C Y, *Int Commun Heat Mass Transfer*, 33 (2006) 627.
20 Gorla R S R, Takhar H S & Slaouti A, *Int J Eng Sci*, 36 (1998) 315.
21 Reddy J N, *An introduction to the finite element method*, (MacGraw-Hill: New York), 1985.
22 Bathe K J, *Finite element procedures*, (Prentice-Hall: New Jersey), 1996.
23 Zaheeruddin K & Isa M, *Wear J*, 51 (1978) 1.
24 Dybbs A & Edwards R V, *NATO*, *ASI series E*, *applied sciences*, (Editors: Bear J & Corapcioglu M Y), 82 (1984).
25 Rees D A S & Pop I, *J Appl Math*, 61 (1998) 179.
26 Rees D A S & Bassom A P, *Int J Eng Sci*, 34 (1996) 113.
27 Chiu C P & Chou H M, *Acta Mechanica*, 101 (1993) 161.
28 Bhargava R, Sharma S, Takhar H S, Bég O A & Bhargava P, *Nonlinear Anal Model Control*, 12 (2007) 45.